A comprehensive experimental and modeling study of the ignition delay time characteristics of ternary and quaternary blends of methane, ethane, ethylene, and propane over a wide range of temperature, pressure, equivalence ratio, and dilution

Combustion and Flame 234 (2021) 111626

Contents lists available at ScienceDirect

Combustion and Flame

journal homepage: www.elsevier.com/locate/combustflame

A comprehensive experimental and modeling study of the ignition delay time characteristics of ternary and quaternary blends of methane, ethane, ethylene, and propane over a wide range of temperature, pressure, equivalence ratio, and dilution

Sergio Martinez[a], Mohammadreza Baigmohammadi[a], Vaibhav Patel[a], Snehasish Panigrahy[a,*], Amrit B. Sahu[a], Shashank Nagaraja[a], Ajoy Ramalingam[b], Karl Alexander Heufer[b], Andrzej Pekalski[c], Henry J. Curran[a]

[a] Combustion Chemistry Centre, School of Chemistry, Ryan Institute, MaREI, National University of Ireland Galway, University Road, Galway H91 TK33, Ireland
[b] Physico-Chemical Fundamentals of Combustion (PCFC), RWTH Aachen University, Aachen 52056, Germany
[c] Shell research limited, Shell Centre London, London SE1 7NA, United Kingdom

ARTICLE INFO

Article history:
Received 21 May 2021
Revised 18 July 2021
Accepted 20 July 2021

Keywords:
Methane
Ethane
Ethylene
Propane
Shock tube
RCM
Ignition delay time

ABSTRACT

The ignition delay time (IDT) characteristics of new ternary and quaternary blended C_1 – C_3 gaseous hydrocarbons, including methane/ethane/ethylene and methane/ethane/ethylene/propane, are studied over a wide range of mixture composition, temperature (~800 – 2000 K), pressure (~1 – 135 bar), equivalence ratio (~0.5 – 2.0), and dilution (~75 – 90%) using both experimental data and kinetic modeling tools. In this regard, all of the experimental tests were designed using the Taguchi approach (L_9) to fulfill the experimental matrix required to generate a comprehensive set necessary to validate a detailed chemical kinetic model. High- and low-temperature IDTs were recorded using low/high-pressure shock tubes (L/HPST) and rapid compression machines (RCM), respectively. The model predictions using NUIGMech1.2 are evaluated versus all of the newly recorded experimental data. Moreover, the individual effects on IDT predictions of the parameters studied, including mixture composition and pressure, are investigated over the temperature range. The results show that NUIGMech1.2 can reasonably reproduce the experimental IDTs over the wide range of the conditions studied. The constant-volume simulations using the chemical kinetic mechanism reveal the synergistic/antagonistic effect of blending on IDTs over the studied temperature range so that IDTs in certain temperature ranges are very sensitive to even small changes in mixture composition.

1. Introduction

The combustion of low-carbon fuels (C_1 – C_3) for energy and power generation is a very promising step towards future low-to-zero emission energy production. Thus, gaining a deep understanding of the combustion chemistry of such fuels and their blends is important. Hence, the development of high-fidelity chemical mechanisms which can satisfactorily explain the oxidation and pyrolytic characteristics of low-carbon fuels is demanding. Together with speciation and laminar burning velocity techniques, ignition delay times (IDTs) are important in the validation of chemical kinetic mechanisms [1, 2]. Developing a comprehensive experimental IDT database that can stochastically and unbiasedly cover a wide range of operating conditions, including pressure, temperature, equivalence ratio, and dilution, is essential in this regard. Such a database can efficiently support the development of high-fidelity chemical kinetics, which can be validated against all available experimental IDT data. To do so, Baigmohammadi et al. [2] studied the IDT characteristics of C_1–C_2 pure hydrocarbons including methane (CH_4), ethane (C_2H_6), and ethylene (C_2H_4) fuels [2] as well as their binary blends [3]. Subsequently Martinez et al. [4] extended this work for higher hydrocarbon by investigating the IDTs of binary blends of C_2H_4/propane (C_3H_8) and C_2H_6/C_3H_8 mixtures in a shock tube (ST) and in a rapid compression machine (RCM) over a wide range of temperature, pressure, equivalence ratio, and dilution conditions.

* Corresponding author.
E-mail address: snehasish.panigrahy@nuigalway.ie (S. Panigrahy).

https://doi.org/10.1016/j.combustflame.2021.111626

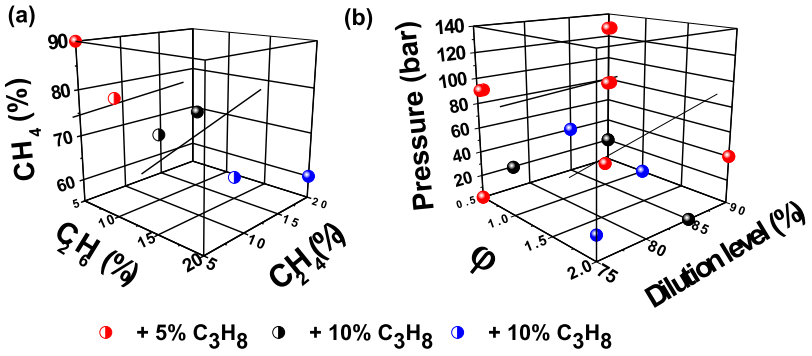

Fig. 1. Experimental tests performed in the current study for% vol. composition of (a) ternary ($CH_4/C_2H_4/C_2H_6$) blends represented in solid symbols and quaternary ($CH_4/C_2H_4/C_2H_6/C_3H_8$) blends represented in half solid symbols, and (b) the input conditions for C_1 – C_3 blends studied in the current work at various equivalence ratios (x-axis), pressures (y-axis) and dilution levels (z-axis).

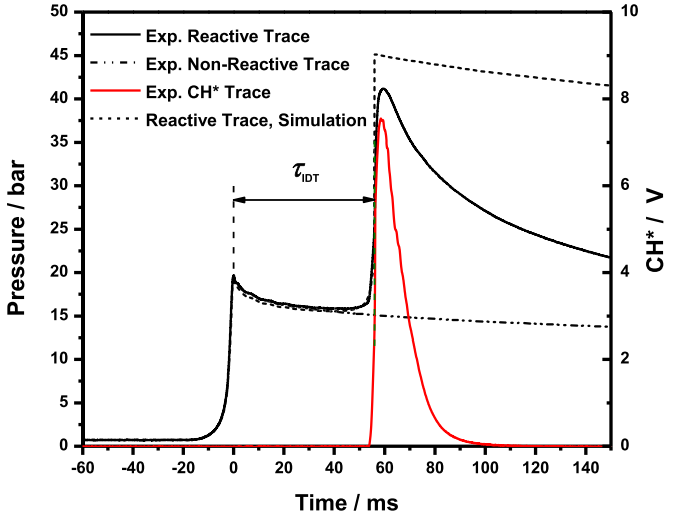

Fig. 2. Definition for measuring IDT in the NUIG-RCM using Kistler pressure trace and PMT-CH* trace mounted on the side wall of the reaction chamber.

As these previous studies focused on the IDT studies of single and binary blended fuel mixtures, *this paper* intends to examine the IDT behaviours of ternary and quaternary blends of C_1 – C_3 hydrocarbons with relevance for engine and gas turbine applications. Furthermore, although there is enough data recorded in the literature for the IDT characteristics of C_1 – C_3 alkane blended fuels and natural gas mixtures (NG) [3-11], evidence of the effect of adding an olefin to C_1 – C_3 alkane blends on IDTs has not been reported to date. Thus, towards developing a comprehensive IDT database, we have designed a set of IDT experiments to cover this void over a wide range of pressure, temperature, equivalence ratio, and dilution (Fig. 1). The new experimental data sets are designed to explore the IDT characteristics of ternary and quaternary blends of $CH_4/C_2H_4/C_2H_6$ and $CH_4/C_2H_4/C_2H_6/C_3H_8$ mixtures.

Furthermore, providing stochastically and unbiasedly distributed experimental IDTs over a wide range of pressure, temperature, equivalence ratio, dilution with varying ethylene concentrations can help researchers develop more sophisticated and higher fidelity chemical kinetics. It can also lead to a valuable database capable of resembling the IDT characteristics of modified NG mixtures for a wide range of applications such as industrial furnaces and internal/external combustion engines working under homogenous charge compression ignition (HCCI), exhaust gas recirculation (EGR), and moderate or intense low oxygen dilution combustion regimes.

To achieve this, the current experimental and simulation study was defined, and the number of desired IDT experiments were optimised, covering the target operating conditions discussed above using the Taguchi [5] design of experiments (DOE) approach as shown in Fig. 1. However, high-pressure (> 40 bar) tests were added to the Taguchi matrix to develop the database further. As shown in Fig. 1(a), the composition of the blends is distributed diagonally to cover the target fuel compositions. Fig. 1(b) demonstrates how using the Taguchi approach, we can reasonably populate the physical conditions in the desired cube so that a wide range of conditions can be covered without performing an overwhelming number of IDT experiments. The designed experiments encapsulate equivalence ratios of 0.5, 1.0, and 2.0 in 'air', at pressures (p_5 and p_C) of 1, 20, 40, 90, and 135 bar, for diluent (N_2 and Ar) concentrations of 75%, 85%, and 90% of reactive mixtures in the temperature (T_5 and T_C) range of ~800 – 2000 K. The detailed kinetic mechanism NUIGMech1.2 is used to evaluate all of the newly measured experimental data, and the important reactions are identified to determine the synergistic/antagonistic effects of various blending effects on the IDTs.

The current study is organized in three stages, including (i) the design of new experiments over a wide range of operating conditions using the Taguchi approach; (ii) experimental measurements; and (iii) simulations using NUIGMech1.2. Comprehensive Supplementary material files containing non-reactive traces for RCM simulations, the original spreadsheets of experimental tests, L/HPST oscilloscope traces, and the combined figures of reactive, non-reactive, and modeling pressure traces are provided along with this paper. Moreover, the general information about the gasses (fuel/oxygen/argon/nitrogen), experimental facilities, and data acquisition systems are also accessible as Supplementary Material.

2. Design of experiments and experimental approach

As mentioned above, all of the new IDT experiments were designed using an L_9 Taguchi matrix to optimally reduce the number of experiments and time required. The Taguchi approach can tackle the issue using a specific design of orthogonal arrays which permits a comprehensive experimental investigation by doing a minimal number of experimental tests. In this regard, the minimum number of experiments is determined as follows:

$$N_{\text{Taguchi}} = 1 + NF\ (L - 1) \quad (1)$$

where, N_{Taguchi}, NF, and L are the number of experiments, number of factors, and number of levels, respectively. According to the Taguchi approach, its performance is optimal when there are limited interactions between the desired variables. To use the Taguchi method, it is essential to define the controlling factors and levels. According to the factors and levels, several design of experiments (DOE) matrices are derived and are included as Supplementary material. The DOE process was followed for four parame-

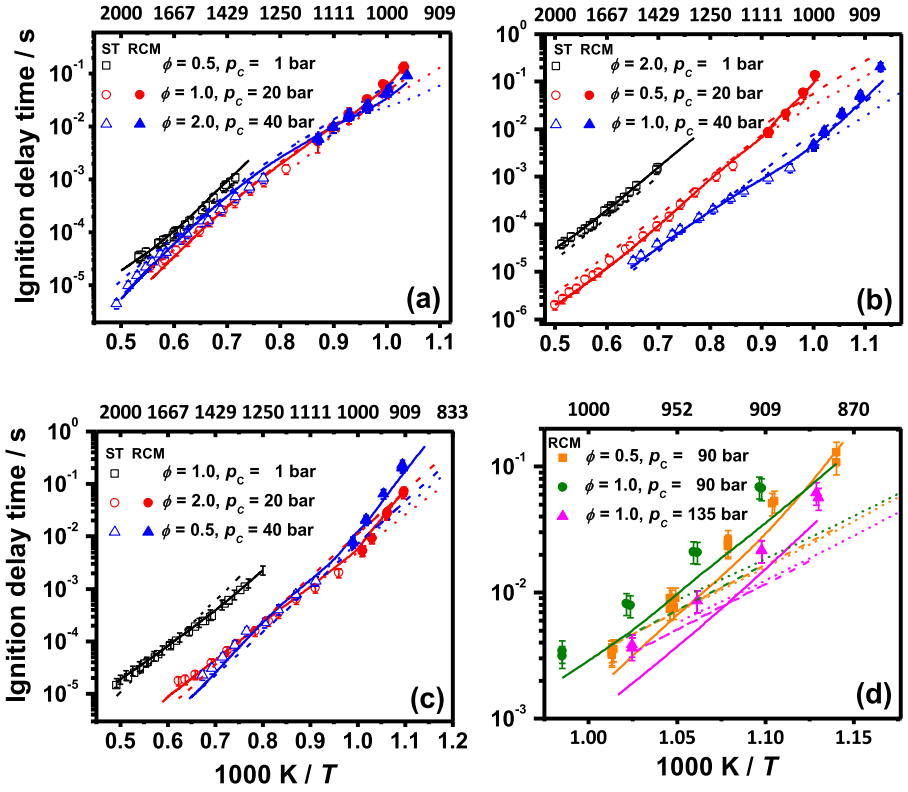

Fig. 3. Experimental and simulated IDT data of $CH_4/C_2H_4/C_2H_6$ mixtures. (a) 90% CH_4/5% C_2H_4/5% C_2H_6 blend at 75% N_2 (black square symbols/lines), 75% N_2+10% Ar (red circle symbols/lines), and 75% N_2+15% Ar (blue triangle symbols/lines), (b) 75% CH_4/12.5% C_2H_4/12.5% C_2H_6 blend at 75% N_2+10% Ar (black square symbols/lines), 75% N_2+15% Ar (red circle symbols/lines), and 75% N_2 (blue triangle symbols/lines), (c) 60% CH_4/20% C_2H_4/20% C_2H_6 blend at 75% N_2+15% Ar (black square symbols/lines), 75% N_2 (red circle symbols/lines), and 75% N_2+10% Ar (blue triangle symbols/lines), (d) 90% CH_4/5% C_2H_4/5% C_2H_6 blend at 90 bar with 67.8% N_2+7.5% Ar (orange square symbols/lines), 68.3% N_2+17% Ar (olive green circle symbols/lines), and at 135 bar with 68.3% N_2+17% Ar (magenta triangle symbols/lines). Solid lines: NUIGMech1.2; dashed lines: derived correlations; and dotted lines: CV – low-temperature simulations. (For interpretation of the references to colour in this figure legend, the reader is referred to the web version of this article.)

ters of ternary and quaternary fuel combinations, pressure, equivalence ratio, and dilution at three levels, where the details are shown in Fig. 1 and Table 1. As previously discussed by Baigmohammadi et al. [2, 3], the new IDT experimental data presented in Table 1 were collected using low- and high-pressure shock tubes (L/HPST) and RCMs refers to the low pressure shock tube, the high pressure shock tube and the (red) rapid compression machine facilities at C^3-NUI Galway, respectively, and PCFC refers to the RCM facility at PCFC RWTH Aachen University.

In the RCM facilities, the IDT of the normal studied mixtures (diluent concentration = 75%) and the pressure/time histories of their relevant non-reactive mixtures were recorded using a Kistler 6045A transducer mounted in the reaction chamber wall. However, the IDTs of mixtures at 85% and 90% dilution and at post-compression pressures of 20 and 40 bar were recorded using both the Kistler pressure record and light emission using a photomultiplier (PMT) equipped with a CH* filter due to the weak pressure signal observed at these diluted conditions. Therefore, as shown in the figure below, the IDT is defined as the maximum gradient in pressure or CH* after compressing the studied mixture. The following figure illustrates the IDT definition for experiments and simulations of the RCM data measured in the current work. More detailed information of the LPST, HPST, NUIG-RCM and PCFC-RCM data is included in Section 5 of the Supplementary material.

2.1. Uncertainty analysis

The details of the uncertainty analysis are provided as Supplementary material. However, a synopsis is presented here. The presented uncertainty analysis is adopted based on the methods applied by Petersen et al. [6] and Weber et al. [7]. According to our analyses [2, 3], the average uncertainties in the compressed mixture temperatures (T_5 or T_C) and measured IDTs (σ_{IDT}%) in the NUIG STs and RCM are estimated to be approximately ± 20 K and ± 25% (in the H/LPSTs) and ± 5 – 15 K and ± 20% (in the RCM), respectively over the entire range of cases studied. The uncertainty in the PCFC RCM is estimated using the methods described in Ramalingam et al. [8], and for the compressed temperature, the uncertainty is estimated to be within ±5 K, with a measurement uncertainty of ± 0.15 bar for the compressed pressure and variation of ± 15% for the IDTs.

3. Computational modeling

NUIGMech1.2 is developed as a further development/refinement of NUIGMech1.1 with the addition and modification of several important reactions which are discussed in more detail in Section 4.2 below. This mechanism includes 2746 species and 11,279 reactions and reproduces similar good results as those previously published using NUIGMech1.1 for the oxidation of C_1 – C_6 species [9-14]. These experimental and theoretical studies include natural gas mixtures [10], propane/propene blends [14], propyne [11], and the auto-ignition and pyrolysis studies of C_2 – C_6 alkenes [12, 13]. All of the simulations are conducted using a Python script based on the CANTERA [15] library for the ST simulation and CHEMKIN-Pro 18.2 [16] software for the RCM simulations. Details of these simulations have already been published [2, 3, 8, 17-20]. The effect of surface reactions on IDTs is ignored in our simulations [2, 3]. The definition of IDT is taken to be the maximum gradient of the CH* species $\frac{dCH^*}{dt}|_{max}$ or the maximum gradient of pressure

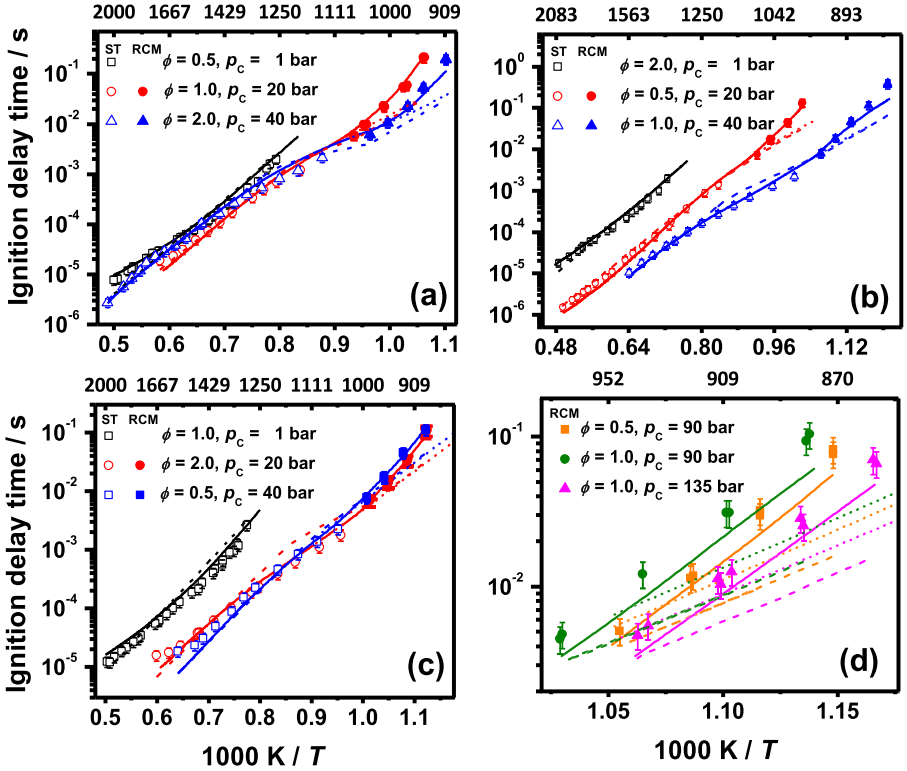

Fig. 4. Experimental and simulated IDT data for $CH_4/C_2H_4/C_2H_6/C_3H_8$ mixtures. (a) 80% CH_4/5% C_2H_4/10% C_2H_6/5% C_3H_8 blend at 75% N_2 (black square symbols/lines), 85% N_2 (red circle symbols/lines), and 90% N_2 (blue triangle symbols/lines), (b) 70% CH_4/10% C_2H_4/10% C_2H_6/10% C_3H_8 blend at 75% N_2+10% Ar (black square symbols/lines), 90% N_2 (red circle symbols/lines), and 75% N_2 (blue triangle symbols/lines), (c) 60% CH_4/15% C_2H_4/15% C_2H_6/10% C_3H_8 blend at 75% N_2+15% Ar (black square symbols/lines), 75% N_2 (red circle symbols/lines), and 85% N_2 (blue triangle symbols/lines), (d) 80% CH_4/5% C_2H_4/10% C_2H_6/5% C_3H_8 blend at 90 bar with 68.1% N_2+7.5% Ar (orange square symbols/lines), 68.5% N_2+17.1% Ar (olive green circle symbols/lines), and at 135 bar with 68.5% N_2+17.1% Ar (magenta triangle symbols/lines). Solid lines: NUIGMech1.2; dashed lines: derived correlations; and dotted lines: CV – low-temperature simulations. (For interpretation of the references to colour in this figure legend, the reader is referred to the web version of this article.)

$\frac{dp}{dt}|_{max}$ for the ST simulations. For the RCM simulations, the facility effects are included using the volume-time profiles derived from the non-reactive experimental pressure-time traces in which O_2 is replaced by N_2 in the mixture [18, 21].

To identify the controlling chemistry both promoting and inhibiting the reactivity of the system and thus their effect on IDT predictions, we present sensitivity analyses based on the brute force definition, with the definition of sensitivity coefficient (S) in Eqn. (2) [22] being:

$$S = \frac{In(\tau+/\tau-)}{In(k+/k-)} = \frac{In(\tau+/\tau-)}{In(2.0/0.5)} \quad (2)$$

This sensitivity coefficient is calculated for every reaction included in the chemical kinetic mechanism of interest. The IDT (τ) is perturbed through direct changes in the pre-exponential factor in the Arrhenius equation. S can be either positive or negative, with a positive value corresponding to a reaction that inhibits reactivity giving longer IDTs and vice versa. Moreover, the flux analyses presented in this work are based on rate of production (ROP) analyses performed to track the consumption of the main components in the different mixture compositions as their intermediates species.

A global analysis of regressions implemented to correlate simulated IDTs assuming constant volume conditions using NUIGMech1.2 is presented in Section 4.4. Moreover, the respective correlation equations and their coefficient values for specific conditions, based on various temperatures, pressure, equivalence ratios, and different fuel mixtures composition, are also provided. General correlations are intended to be a practical engineering tool to quickly and accurately calculate IDTs at the required condition. A more complete and fully detailed Tables S12 – S15 of correlation values, standard errors, and performance are included as Supplementary material.

4. Results and discussions

A comprehensive comparison between the experimental IDTs (Table 1) and those predicted using NUIGMech1.2 is presented below.

4.1. Performance of NUIGMech1.2 and the correlations versus experimental data

The performance of NUIGMech1.2 compared to the new experimental ST and RCM IDT data for various ternary and quaternary blends of $CH_4/C_2H_4/C_2H_6$ and $CH_4/C_2H_4/C_2H_6/C_3H_8$ fuels, Table 1, is shown in Figs. 3 and 4. The symbols refer to the experimental data, with the solid lines from NUIGMech1.2 simulations and the dashed lines representing the correlation equation results. These correlations are derived over well-defined conditions, as discussed in Section 4.4.

Figs. 3 and 4 show that NUIGMech1.2 can reasonably reproduce all of the measured IDTs over the stochastically distributed conditions studied. It not only reproduces the effects of mixture composition and temperature on IDTs, but it can also reliably predict the effects of pressure, equivalence ratio, and the effect of dilution except at very high-pressures ($\geq$ 90 bar) where the model underpredicts the IDTs for the ternary blends of the $CH_4/C_2H_4/C_2H_6$ mixtures. A detailed comparison between the performance of NUIGMech1.2 and other available mechanisms is provided in Section 9

Table 1
$CH_4/C_2H_4/C_2H_6$ and $CH_4/C_2H_4/C_2H_6/C_3H_8$ mixture compositions in% mole volume in the current study. Where keywords LPST, HPST and RCM.

	No	% CH_4	% C_2H_4	% C_2H_6	% C_3H_8	% O_2	% N_2 +% Ar	φ	T_C (K)	p_C (bar)	*Facility*
$CH_4/C_2H_4/C_2H_6$	1	4.29	0.24	0.24	0.0	20.24	75+0	0.5	1396–1874	1	LPST NUIG
90%/5%/5%	2	4.32	0.24	0.24	0.0	10.20	75+10	1.0	967–1797	20	HPST
	3	4.40	0.20	0.20	0.0	5.20	75+15	2.0	960–2033	40	RCM
CH_4/75.3%C_2H_4/C_2H_6	4	5.70	0.90	0.90	0.0	17.50	75+0	1.0	885–1536	40	NUIG
75%/12.5%/12.5%	5	5.22	0.87	0.87	0.0	8.04	75+10	2.0	1432–1951	1	LPST NUIG
	6	1.33	0.22	0.22	0.0	8.22	75+15	0.5	996–2001	20	HPST
$CH_4/C_2H_4/C_2H_6$	7	6.67	2.22	2.22	0.0	13.89	75+0	2.0	911–1604	20	RCM
60%/20%/20%	8	1.5	0.50	0.50	0.0	12.50	75+10	0.5	914–1484	40	NUIG
	9	1.71	0.57	0.57	0.0	7.14	75+15	1.0	1311–2032	1	LPST NUIG
$CH_4/C_2H_4/C_2H_6$	10	4.24	0.24	0.24	0.0	20	67.8 + 7.5	0.5	877–987	90	RCM
90%/5%/5%	11	4.24	0.24	0.24	0.0	10	68.3 + 17	1.0	885–976	135	PCFC
	12	4.24	0.24	0.24	0.0	10	68.3 + 17	1.0	911–1015	90	
$CH_4/C_2H_4/C_2H_6/C_3H_8$	13	3.51	0.22	0.44	0.22	20.61	75+0	0.5	1259–2002	1	LPST NUIG
80%/5%/10%/5%	14	3.58	0.22	0.45	0.22	10.50	85+0	1.0	941–1717	20	HPST
	15	3.68	0.23	0.46	0.23	5.40	90+0	2.0	908–2049	40	RCM
$CH_4/C_2H_4/C_2H_6/C_3H_8$	16	4.93	0.70	0.70	0.70	17.96	75+0	1.0	826–1561	40	NUIG
70%/10%/10%/10%	17	4.62	0.66	0.66	0.66	8.41	75+10	2.0	1379–2062	1	LPST NUIG
	18	1.15	0.16	0.16	0.16	8.36	90+0	0.5	977–2024	20	HPST
$CH_4/C_2H_4/C_2H_6/C_3H_8$	19	6.42	1.60	1.60	1.07	14.30	75+0	2.0	890–1668	20	RCM
60%/15%/15%/10%	20	1.41	0.35	0.35	0.24	12.64	85+0	0.5	891–1560	40	NUIG
	21	1.63	0.41	0.41	0.27	7.28	75+15	1.0	1290–1987	1	LPST NUIG
$CH_4/C_2H_4/C_2H_6/C_3H_8$	22	3.42	0.21	0.43	0.21	20.10	68.1 + 7.5	0.5	871–948	90	RCM
80%/5%/10%/5%	23	3.43	0.21	0.43	0.21	10.08	68.5 + 17.1	1.0	857–941	135	PCFC
	24	3.43	0.21	0.43	0.21	10.08	68.5 + 17.1	1.0	879–972	90	

of the Supplementary material. Considering similar comparisons of C_1 – C_3 pure and binary fuels mixtures, including methane, ethane, ethylene, and propane, over the wide range of physical and chemical conditions presented previously by the authors [2-4], NUIGMech1.2 better reproduces the oxidation behavior of small hydrocarbon species compared to other similar available mechanisms [23-32].

4.2. Effect of blending on ignition

To determine the chemistry controlling ignition times of $CH_4/C_2H_4/C_2H_6$/'air' and $CH_4/C_2H_4/C_2H_6/C_3H_8$/'air' blends, Fig. 5(a) depicts the IDTs of single fuel mixtures of CH_4/'air', C_2H_4/'air', C_2H_6/'air', C_3H_8/'air', while binary mixtures of CH_4/C_2H_6/'air' are depicted together with the ternary and quaternary blends at fuel-stoichiometric condition, at a pressure of 40 atm and temperatures in the range 714 – 1667 K.

At first glance, in Fig. 5(a), the CH_4/'air' mixture is the slowest to ignite over the entire temperature range studied in this work, while the C_2H_6/'air' is the next slowest in the low-temperature regime ($<$ 900 K), being ~25% faster than CH_4. However, C_2H_6/'air' becomes the second-fastest mixture to ignite, after ethylene, by inverting its trend at $\sim T_C$ = 1100 K. Overall, C_2H_6/'air' mixtures are approximately an order of magnitude faster to ignite than CH_4 and are ~50% faster compared to the C_3H_8/'air' mixtures, but are slower by a factor of ~1.5 when compared to C_2H_4/'air' mixtures at temperatures higher than 1150 K. The C_2H_4/'air' mixtures are the fastest to ignite at high-temperatures, and exhibit shorter IDTs compared to the C_3H_8/'air' mixtures at temperatures below ~1050 K, with propane being the fastest fuel to ignite in the low-temperature regime.

To determine the chemistry controlling the reactivities of various fuel/'air' mixtures, reaction pathways based on multiple rate of production (ROP) analyses are illustrated in Fig. 6 for (i) the pure fuels in 'air', (ii) the 50% CH_4/50% C_2H_6 binary mixtures, (iii) the 50% CH_4/25% C_2H_4/25% C_2H_6/ ternary mixtures, and (iv) the 50% CH_4/16.66% C_2H_4/16.66% C_2H_6/16.66% C_3H_8 quaternary mixtures at p_C = 40 atm, φ = 1.0, for (a) T_C = 800 K and (b) T_C = 1450 K. The ROP analyses are implemented following a standardized elemental carbon balance. The normalised values above the arrow denote the fractions of the parent fuel proceeding via various reaction pathways. Moreover, sensitivity analyses are performed at p_C = 40 atm, φ = 1.0, for (a) T_C = 800 K and (b) T_C = 1450 K to interpret the most sensitive reactions to IDTs and are presented in Fig. 7.

Fig. 7(b) shows that, at 1450 K, the chain branching reaction $\dot{H} + O_2 \leftrightarrow \ddot{O} + \dot{O}H$ governs and promotes the ignition of the fuel/'air' mixtures, the rate of which depends on the amount of hydrogen atoms and molecular oxygen available in the mixtures. However, for the CH_4/'air' mixture, methyl ($\dot{C}H_3$) radicals rather than $\dot{H}$ atoms dominate the ignition behavior, with $\dot{C}H_3 + H\dot{O}_2 \leftrightarrow CH_3\dot{O} + \dot{O}H$ and $\dot{C}H_3 + \dot{O}_2 \leftrightarrow CH_2O + \dot{O}H$ being the most sensitive reactions promoting reactivity, and $\dot{C}H_3 + \dot{C}H_3 (+M) \leftrightarrow C_2H_6 (+M)$ is the most sensitive reaction inhibiting reactivity, as illustrated in Fig. 7(b). At 1450 K, CH_4 is mostly consumed by H-atom abstraction by $\dot{H}$, $\ddot{O}$ and $\dot{O}H$ radicals producing methyl ($\dot{C}H_3$) radicals, Fig. 6(b). Approximately 11% of these $\dot{C}H_3$ radicals react with O_2 through $\dot{C}H_3 + O_2 \leftrightarrow CH_2O + \dot{O}H$ to generate formaldehyde (CH_2O) and $\dot{O}H$ radicals in a reaction that greatly promotes the reactivity of the mixture, as seen by the sensitivity analysis presented in Fig 7(b). The CH_2O then reacts with $\dot{C}H_3$ radical and leads to the formation of CH_4 and formyl ($H\dot{C}O$) radical. Another pathway contributing to the consumption of the $\dot{C}H_3$ radicals (15.8%) is the chain branching reaction $\dot{C}H_3 + H\dot{O}_2 \leftrightarrow CH_3\dot{O} + \dot{O}H$, which produces methoxy ($CH_3\dot{O}$) and $\dot{O}H$ radicals, significantly promoting reactivity, Figs. 6(b) and 7(b). The current mechanism employs the rate coefficients for $\dot{C}H_3 + H\dot{O}_2 \leftrightarrow CH_3\dot{O} + \dot{O}H$ from the theoretical calculation by Jasper et al. [33]. This reaction channel directly competes with the chain-terminating reaction $\dot{C}H_3 + H\dot{O}_2 \leftrightarrow CH_4 + O_2$ for hydroperoxyl ($H\dot{O}_2$) radicals, as shown in Fig. 7(b), and the current mechanism utilizes the rate constant from Zhu et al. [34] for this inhibiting pathway. At the high temperature of 1450 K, ~7% of methyl ($\dot{C}H_3$) radicals react with O_2 to form methyl peroxy ($CH_3\dot{O}_2$) radicals via $\dot{C}H_3 + O_2 \leftrightarrow CH_3\dot{O}_2$. These radicals further dissociate to CH_2O and $\dot{O}H$ radicals, promoting reactivity as illustrated in Fig 7(b). This direct dissociation of $CH_3\dot{O}_2$ radicals was not incorporated in the previous mechanism, and in NUIGMech1.2, the rate constant for this reaction is adopted based on an extensive study of rate rules by Villano et al. [35] derived using electronic structure calculations.

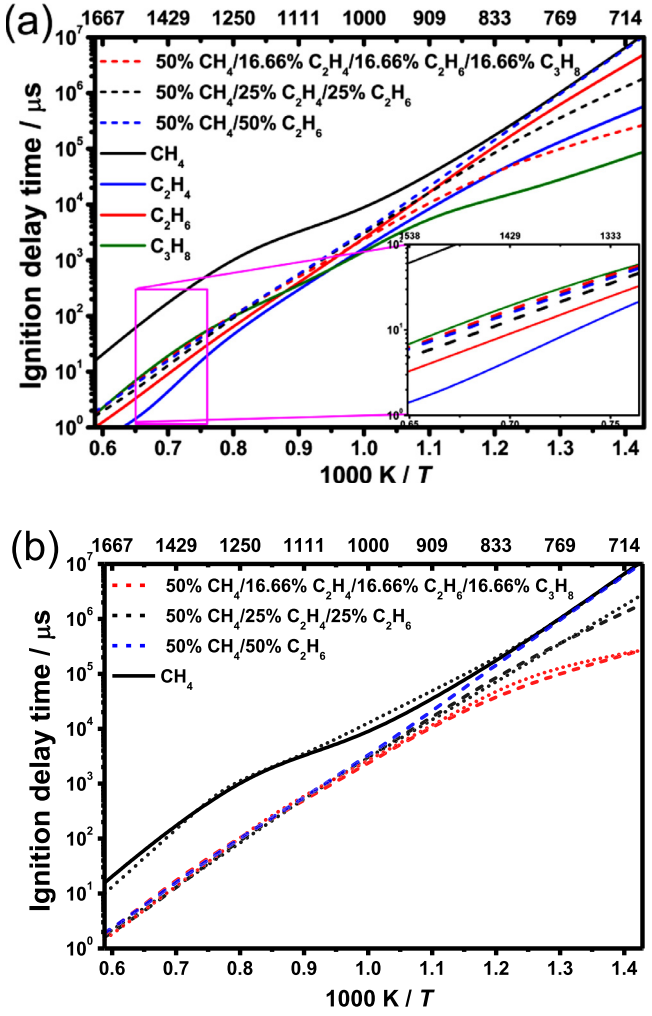

Fig. 5. (a) Comparisons of IDT predictions for various single, binary, ternary, and quaternary fuels in air at p_C = 40 atm and φ = 1.0, and (b) the predictions of their corresponding correlations (dotted lines). (For interpretation of the references to colour in this figure legend, the reader is referred to the web version of this article.)

Fig. 8(a) shows the importance of the addition of the $CH_3\dot{O}_2$ dissociation channel and the updated rate constant for $\dot{C}H_3 + \dot{C}H_3$ $(+M) \leftrightarrow C_2H_6$ $(+M)$ on the IDT predictions using NUIGMech1.2 compared to NUIGMech1.1, which slightly under-predicts the IDTs in the intermediate temperature range of 1000 – 1100 K at p_C = 24 atm, and for both φ = 0.5 and 1.0. The addition of the $CH_3\dot{O}_2 \leftrightarrow CH_2O + \dot{O}H$ reaction channel results in a decrease in predicted IDTs represented by dashed-dotted lines in Fig. 8(a). Nonetheless, an excellent improvement in IDT prediction is achieved by updating the $\dot{C}H_3 + \dot{C}H_3$ $(+M) \leftrightarrow C_2H_6$ $(+M)$ rate constants together with the inclusion of the $CH_3\dot{O}_2$ dissociation reaction ($CH_3\dot{O}_2 \leftrightarrow CH_2O + \dot{O}H$) in NUIGMech1.2, as depicted by the solid lines in Fig. 8(a).

According to the ROP and the sensitivity analysis of CH_4/'air' mixtures, at high temperatures (1450 K) a significant quantity (~55%) of the methyl radicals undergo self-recombination to form C_2H_6 making methane the slowest fuel to ignite compared to the other single fuels. The self-recombination reaction of methyl radicals has been widely studied in the literature. Comparisons of pressure-dependent rate constants and various experimental measurements for $\dot{C}H_3 + \dot{C}H_3$ $(+M) \leftrightarrow C_2H_6$ $(+M)$ from the literature [37-42] are shown in Fig. 8(b). NUIGMech1.1 employed a rate constant from the experimental and theoretical study of Wang et al. [41] for this reaction. Here NUIGMech1.2 uses the fit derived from

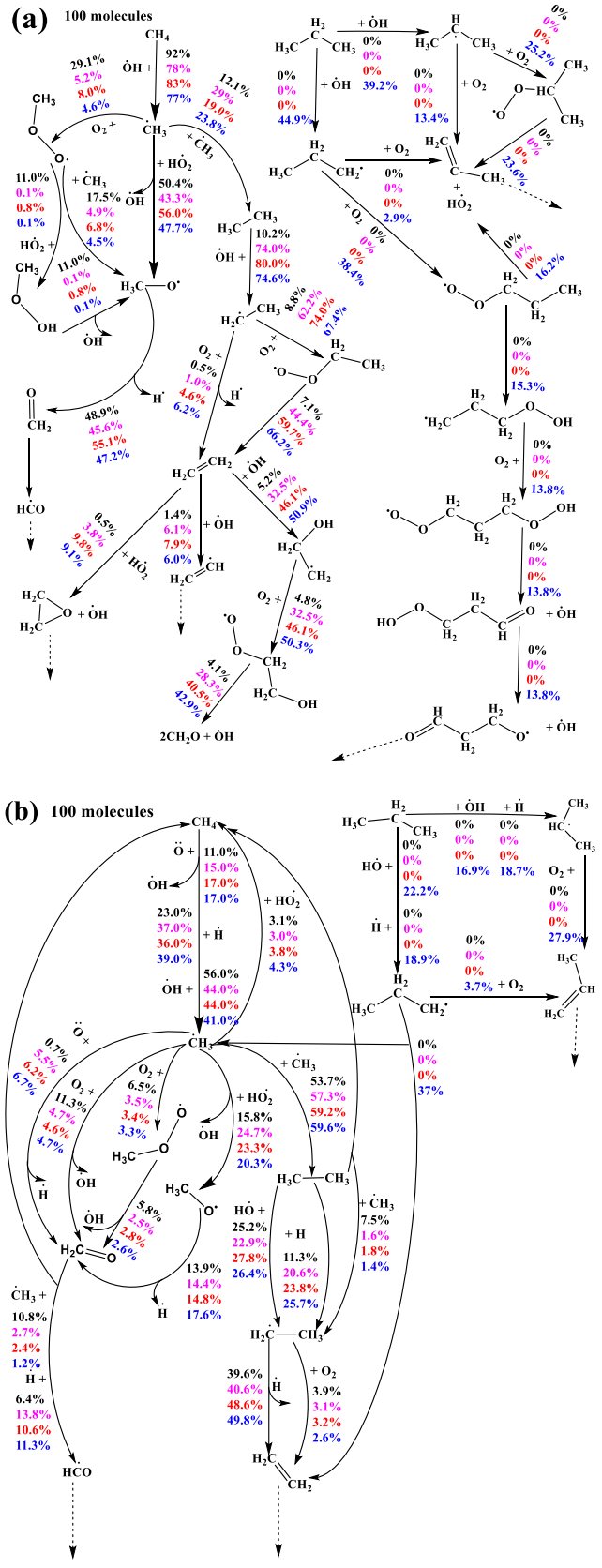

Fig. 6. Flux analyses of pure CH_4 (black), 50% CH_4/50% C_2H_6 blend (magenta), 50% CH_4/25% C_2H_4/25% C_2H_6 blend (red), and 50% CH_4/16.66% C_2H_4/16.66% C_2H_6/16.66% C_3H_8 (blue) mixtures at p_C = 40 atm and φ = 1.0, at the time of 20% fuel consumed for (a) T_C = 800 K and (b) T_C = 1450 K. (For interpretation of the references to colour in this figure legend, the reader is referred to the web version of this article.)

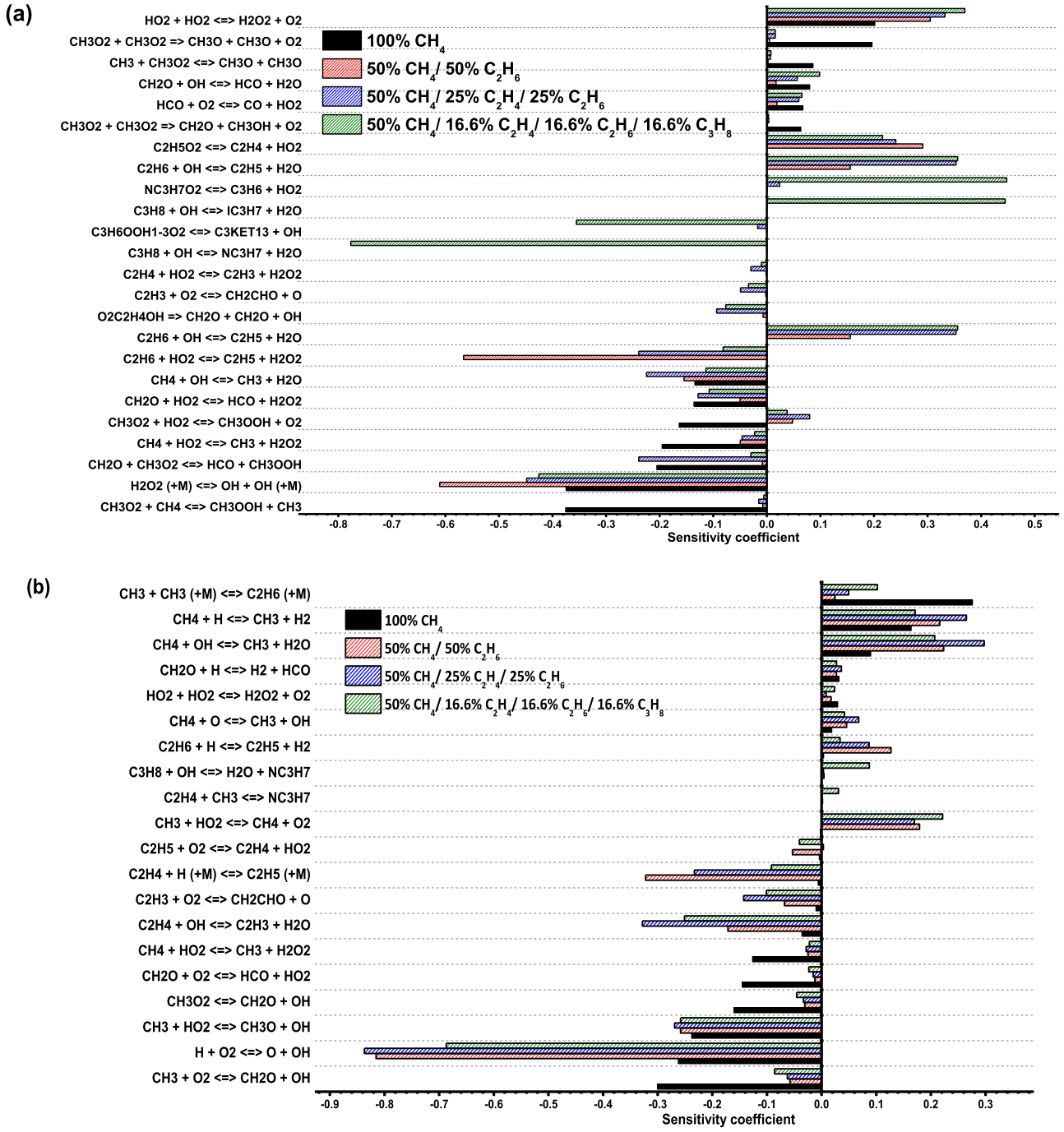

Fig. 7. Sensitivity analyses to IDTs for pure CH_4, 50% CH_4/50% C_2H_6 blend, 50% CH_4/25% C_2H_4/25% C_2H_6 blend, and 50% CH_4/16.66% C_2H_4/16.66% C_2H_6/16.66% C_3H_8 mixtures in 'air' at $p_C = 40$ atm, $\varphi = 1.0$, for (a) $T_C = 800$ K and (b) $T_C = 1450$ K.

a comprehensive experimental review by Blitz et al. [40] for the high-pressure limit rate constant. We have chosen this rate constant as the revised high-pressure limit is in good agreement with the recent experimental study by Sangwan et al. [38] in the temperature range 292 – 714 K as well as with the high level theoretical calculation by Klippenstein et al. [42]. Fig. 8(b) shows that the high-pressure limit reported by Wang et al. [41] is ∼17% slower than that measured by Sangwan et al. [38] at 714 K. In NUIG-Mech1.2 the low-pressure limit and the fall-off parameters are taken from Wang et al. [41], as these satisfactory match the experimental measurements from Slagle et al. [37] and Glanzer et al. [39] in the pressure-dependent fall-off regime, Fig. 8(b).

In Fig. 6(a), the ROP analysis of the pure CH_4/'air' mixture at 800 K shows that ∼50% of $\dot{C}H_3$ radicals react with $H\dot{O}_2$ forming methoxy ($CH_3\dot{O}$) radicals by $\dot{C}H_3 + H\dot{O}_2 \leftrightarrow CH_3\dot{O} + \dot{O}H$, which further decomposes through $CH_3\dot{O}\ (+M) \leftrightarrow CH_2O + \dot{H}\ (+M)$ to produce formaldehyde (CH_2O) and $\dot{H}$ atoms. A significant quantity of $\dot{C}H_3$ (30%) reacts with O_2 to form methyl peroxy radicals through $\dot{C}H_3 + O_2 \leftrightarrow CH_3\dot{O}_2$. Approximately ∼11% of $CH_3\dot{O}_2$ is consumed by its reaction with $H\dot{O}_2$, via $CH_3\dot{O}_2 + H\dot{O}_2 \leftrightarrow CH_3OOH + O_2$ followed by rapid dissociation of the methyl hydroperoxide (CH_3OOH) into methoxy ($CH_3\dot{O}$) and $\dot{O}H$ radicals, thus significantly enhancing reactivity. Furthermore, considerable amounts of CH_3OOH can be produced from $CH_3\dot{O}_2$ by $CH_3\dot{O}_2 + CH_4 \leftrightarrow CH_3OOH + \dot{C}H_3$ and

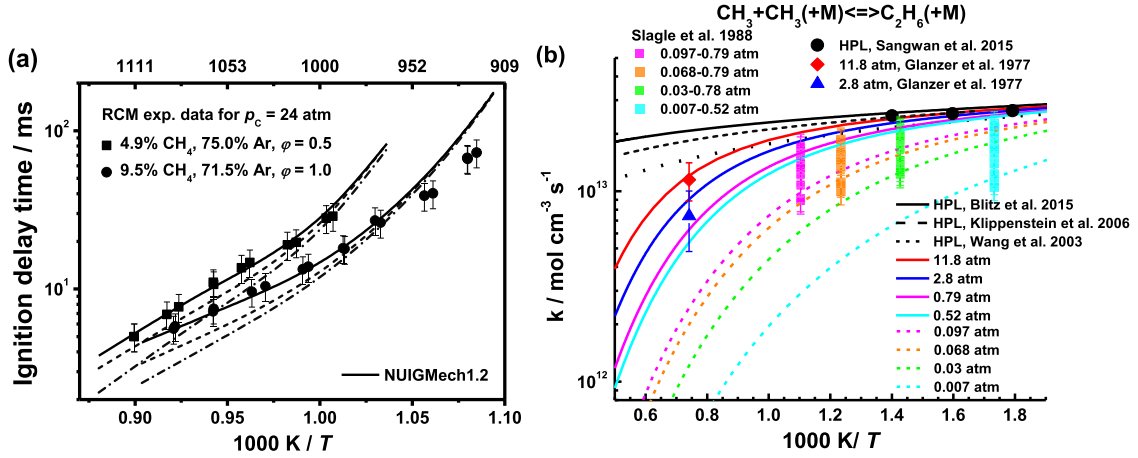

Fig. 8. (a) Effects of addition of $CH_3\dot{O}_2 \leftrightarrow CH_2O + \dot{O}H$ reaction and updated $\dot{C}H_3+\dot{C}H_3$ $(+M) \leftrightarrow C_2H_6$ $(+M)$ rate constant on the IDTs for 4.9% CH_4 at φ = 0.5 [36] and 9.5% CH_4 at φ=1.0 [36]; ——, NUIGMech1.1; – • – •, NUIGMech1.1 plus $CH_3\dot{O}_2 \leftrightarrow CH_2O + \dot{O}H$ [35]; – – –, NUIGMech1.2 which includes $CH_3\dot{O}_2 \leftrightarrow CH_2O + \dot{O}H$ [35] reaction as well as an updated rate constant for $\dot{C}H_3 + \dot{C}H_3$ $(+M) \leftrightarrow C_2H_6$ $(+M)$. (b) Comparisons of the rate constants for $\dot{C}H_3 + \dot{C}H_3$ $(+M) \leftrightarrow C_2H_6$ $(+M)$ [37-42].

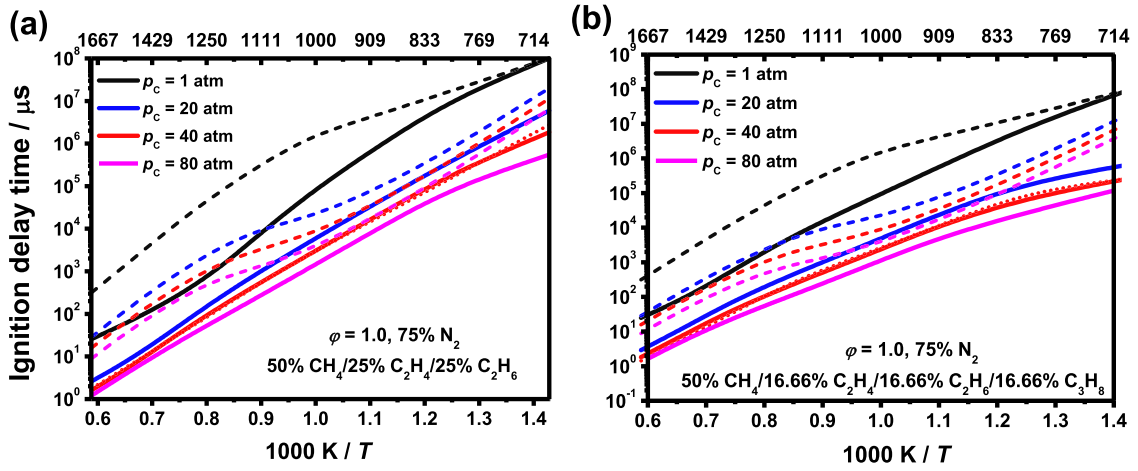

Fig. 9. Effect of pressure over the IDT predictions of (a) 50% CH_4/25% C_2H_4/25% C_2H_6 blend (solid lines), and (b) 50% CH_4/16.66% C_2H_4/16.66% C_2H_6 /16.66% C_3H_8 blend (solid lines), pure CH_4 (dashed lines), and corresponding correlations (dotted lines) for fuel in air at φ = 1.0. (For interpretation of the references to colour in this figure legend, the reader is referred to the web version of this article.)

$CH_2O + CH_3\dot{O}_2 \leftrightarrow HCO + CH_3OOH$ reactions promoting methane ignition at low temperatures, as can be seen in Fig. 7(a). The ROP analysis shows that ~17% of $CH_3\dot{O}_2$ radicals further react with $\dot{C}H_3$ to produce two methoxy radicals through $CH_3\dot{O}_2 + \dot{C}H_3 \leftrightarrow CH_3\dot{O} + CH_3\dot{O}$. Fig. 7(a) also shows that this reaction along with $CH_3\dot{O}_2 + CH_3\dot{O}_2 \leftrightarrow CH_3\dot{O} + CH_3\dot{O} + O_2$ competes for $CH_3\dot{O}_2$ radicals with the chain propagating reactions $CH_4 + CH_3\dot{O}_2 \leftrightarrow CH_3OOH + \dot{C}H_3$ and $CH_2O + CH_3\dot{O}_2 \leftrightarrow H\dot{C}O + CH_3OOH$ producing methyl hydroperoxide, thus decreasing the reactivity of the CH_4/'air' mixture. NUIGMech1.2 utilizes the rate constant recommended by Lightfoot et al. [43] for $CH_3\dot{O}_2 + CH_3\dot{O}_2 \leftrightarrow CH_3\dot{O} + CH_3\dot{O} + O_2$ based on flash photolysis measurements at atmospheric and low temperatures conditions, as shown in Fig. S51. For $CH_3\dot{O}_2 + \dot{C}H_3 \leftrightarrow CH_3\dot{O} + CH_3\dot{O}$, the rate coefficients are adopted from the work of Keiffer et al. [44], as shown in Fig. S52. However, further research is recommended in the study of the rate constant of this reaction. Finally, at 800 K, the remaining 12% of $\dot{C}H_3$ radicals react through the self-recombination reaction $\dot{C}H_3 + \dot{C}H_3$ $(+M) \leftrightarrow C_2H_6$ $(+M)$, thus activating the C_2H_6 chemistry.

Unlike the case for CH_4/'air' mixtures, the most important reaction promoting the reactivity at high temperatures for the binary, ternary and quaternary blends is the chain branching reaction $\dot{H} + O_2 \leftrightarrow \ddot{O} + \dot{O}H$. This is because C_2H_4, C_2H_6, and C_3H_8 mixtures generate larger concentrations of $\dot{H}$ atoms compared to CH_4/'air' mixtures and consequently increases the fuel reactivities of the blended mixtures at the high-temperature conditions, as shown in Fig. 5. In a previous study [4], the important reactions, as well as the choice of their rate constants governing the oxidation behavior of C_2H_4/'air', C_2H_6/'air', C_3H_8/'air' mixtures and their binary blends, were discussed in detail. Thus, in this work, particular emphasis is placed on understanding the synergistic and antagonistic effects of ethane/ethylene/propane fuels on the ignition of methane/fuel mixtures.

The consumption of C_2H_6 is initiated by H-atom abstraction, mainly by $\dot{O}H$ radicals and $\dot{H}$ atoms producing ethyl radicals ($\dot{C}_2H_5$), through $C_2H_6 + \dot{H}/\dot{O}H \leftrightarrow \dot{C}_2H_5 + H_2/H_2O$. Most ethyl radicals decompose to C_2H_4 and $\dot{H}$ atoms via $\dot{C}_2H_5$ $(+M) \leftrightarrow C_2H_4 + \dot{H}$ $(+M)$. Ethylene can further undergo H-atom abstraction reactions to form vinyl radicals ($\dot{C}_2H_3$) which are responsible for the generation of a substantial amount of $\dot{H}$ atoms by their reaction with O_2 via $\dot{C}_2H_3 + O_2 \leftrightarrow \dot{C}H_2CHO + \ddot{O}$ and $CH_2CHO \leftrightarrow CH_2CO + \dot{H}$, ultimately leading to the faster ignition of C_2H_6/air mixtures compared to CH_4/air mixtures, as shown in Fig 5(a). The remaining $\dot{C}_2H_5$ radicals react with O_2 to produce ethylene through $\dot{C}_2H_5 + O_2 \leftrightarrow C_2H_4 + H\dot{O}_2$, which directly competes with $\dot{C}_2H_5$ $(+M) \leftrightarrow C_2H_4 + \dot{H}$ $(+M)$, resulting in a shorter IDT for C_2H_6/air

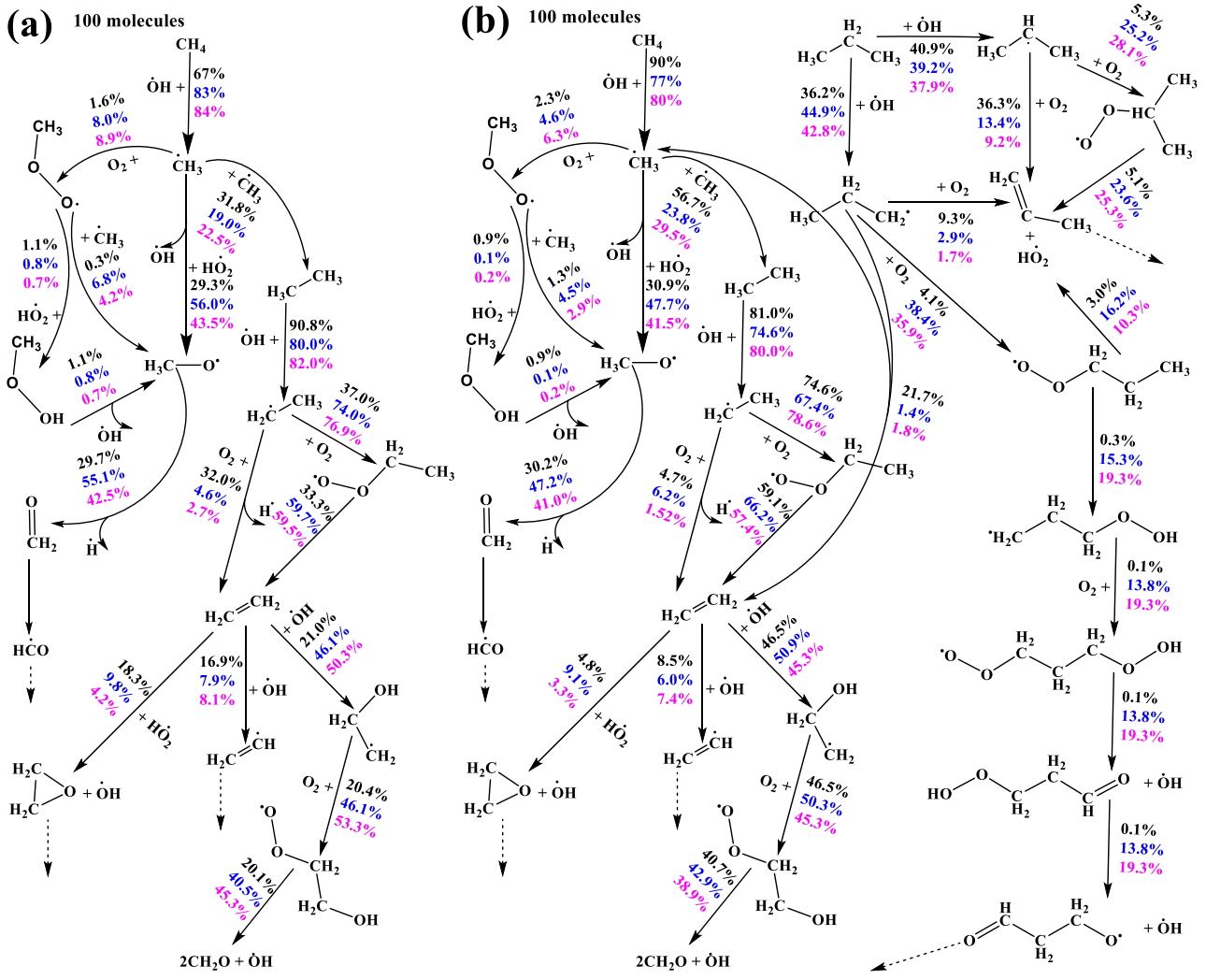

Fig. 10. Flux analyses as function of pressure of 1 atm, 40 atm and 80 atm (black, blue, and magenta percentages respectively), at T_C = 800 K, φ = 1.0, for (a) 50% CH_4/25% C_2H_4/25% C_2H_6, and (b) 50% CH_4/16.66% C_2H_4/16.66% C_2H_6/16.66% C_3H_8 in air. (For interpretation of the references to colour in this figure legend, the reader is referred to the web version of this article.)

mixture compared to C_2H_4/air mixture. The effect on IDTs of the addition of ethane to CH_4/air mixtures is presented in Fig 5(a). The reactivity of the mixture increases significantly for the 50% CH_4/50% C_2H_6 binary blend at high temperatures (> 1000 K) compared to the pure methane mixture. In Fig. 6(b), the magenta-bold percentages represent the ROP for 50% CH_4/50% C_2H_6 binary mixtures at 40 atm, φ = 1.0 and T_C = 1450 K. Flux analyses show that the addition of C_2H_6 to CH_4/air mixtures does not alter the main reaction pathways corresponding to the pure CH_4 chemistry; however, it leads to increased production of Ḣ atoms which increases the sensitivity coefficients of Ḣ + O_2 ↔ Ö + ȮH and C_2H_4 + ȮH ↔ $\dot{C}_2H_3$ + HȮ$_2$ for the 50% CH_4/50% C_2H_6 binary mixtures, Fig. 7(b). On the contrary, the reactions CH_4 + Ḣ ↔ $\dot{C}H_3$ + H_2 and CH_4 + ȮH ↔ $\dot{C}H_3$ + H_2O compete for the available Ḣ atoms and ȮH radicals which exhibit higher positive sensitive coefficients for the C_2H_6 blended mixtures in comparison to the pure CH_4 case.

At low temperatures, the pure C_2H_6/air mixture is still faster to ignite compared to the pure CH_4/'air' mixture, but the difference between the two decreases with a decrease in temperature, Fig. 5(a). Furthermore, for the 50% CH_4/50% C_2H_6 binary blend, the IDT predictions overlap with the pure CH_4 ones at low-temperatures. The sensitivity analysis shows that the sensitivities of H_2O_2 (+M) ↔ ȮH + ȮH (+M) and HȮ$_2$ + HȮ$_2$ ↔ H_2O_2 + O_2 are strengthened by the addition of 50% C_2H_6 to CH_4/air mixtures. This is because, compared to the pure CH_4 case, H-atom abstraction from C_2H_6 by HȮ$_2$ radicals exhibits a relatively larger negative sensitivity coefficient promoting reactivity, which is attributed to the higher rate constant of C_2H_6 + HȮ$_2$ ↔ $\dot{C}_2H_5$ + H_2O_2, which is approximately an order of magnitude faster than that for CH_4 + HȮ$_2$ ↔ $\dot{C}H_3$ + H_2O_2. However, most of the $\dot{C}_2H_5$ radicals formed add to O_2 producing ethylperoxy ($C_2H_5\dot{O}_2$) radicals, followed by the concerted elimination reaction $C_2H_5\dot{O}_2$ ↔ C_2H_4 + HȮ$_2$, which plays an important role in inhibiting the ignition of the C_2H_6 blended mixtures at low temperatures, Fig. 7(a).

C_2H_4 is an essential intermediate of C_2H_6 oxidation and is the fastest fuel to ignite compared to the other single fuels at high temperatures. The effect on IDT predictions of the addition of C_2H_4 to a CH_4/C_2H_6/'air' mixture is presented in Fig 5(a). The reactivity of the 50% CH_4/25% C_2H_6/25% C_3H_8 ternary blend is ~15% faster than the CH_4/C_2H_6 binary blend at high temperatures (> 1000 K). Moreover, at low temperatures, the ternary blend is ~80% faster than the binary blend. The main reason for the increased reactivity of C_2H_4 blended mixtures at high temperatures is attributed to the substantial formation of Ḣ atoms due to the reaction sequence, C_2H_4 + Ö ↔ $\dot{C}H_2CHO$ + Ḣ, and C_2H_4 + Ö ↔ C̈H$_2$ + CH_2O, followed by C̈H$_2$ + O_2 ↔ CO_2 + Ḣ + Ḣ [4], thus increasing the im-

portance of the $\dot{H} + O_2 \leftrightarrow \ddot{O} + \dot{O}H$ and $C_2H_4 + \dot{O}H \leftrightarrow \dot{C}_2H_3 + H\dot{O}_2$ reactions for the ternary blend compared to the binary blend mixtures, Fig. 7(b). On the other hand, at low temperatures (< 1000 K), C_2H_4 is primarily consumed by the addition of $\dot{O}H$ radicals producing hydroxyl–ethyl ($\dot{C}_2H_4OH$) radicals which add to molecular oxygen to form hydroxyethylene-peroxy ($\dot{O}_2C_2H_4OH$) radicals. The dissociation of $\dot{O}_2C_2H_4OH$ radicals ultimately increases the reactivity of the ethylene blended mixtures at low temperatures by generating two molecules of formaldehyde and $\dot{O}H$ radicals. For the ternary mixtures, $\dot{O}H$ radicals are also formed through the reaction $C_2H_4 + H\dot{O}_2 \leftrightarrow C_2H_4O1\text{–}2$ (oxirane) + $\dot{O}H$, further promoting reactivity.

Propane/'air' oxidation at high temperatures (> 900 K) is mainly dominated by H-atom abstraction by $\dot{O}H$ radicals and $\dot{H}$ atoms, leading to the formation of *n*-propyl ($n\dot{C}_3H_7$) and isopropyl ($i\dot{C}_3H_7$) radicals. Most $n\dot{C}_3H_7$ radicals decompose via β-scission $n\dot{C}_3H_7 \leftrightarrow C_2H_4 + \dot{C}H_3$. The methyl radicals so formed can react with hydroperoxyl radicals either via $\dot{C}H_3 + H\dot{O}_2 \leftrightarrow CH_3\dot{O} + \dot{O}H$, which promotes reactivity, or $\dot{C}H_3 + H\dot{O}_2 \leftrightarrow CH_4 + O_2$, which inhibits reactivity. Methyl radicals also self-react to form C_2H_6, further reducing the reactivity of the propane/air mixtures. The effect on IDTs of adding C_3H_8 to $CH_4/C_2H_6/C_2H_4$/'air' mixtures is shown in Fig 5(a). At high temperatures, the 50% CH_4/16.66% C_2H_6/16.66% C_2H_4/16.66% C_3H_8 quaternary blend is ~15% slower than the 50% CH_4/25% C_2H_6/25% C_3H_8 ternary mixtures, Fig 5(a). The sensitivity analysis, Fig. 7(b), shows that at 1450 K, the main chain branching reaction $\dot{H} + O_2 \leftrightarrow \ddot{O} + \dot{O}H$ is relatively less sensitive to the IDT of the quaternary blends compared to the ternary blends leading to a lower reactivity of the 50% CH_4/16.66% C_2H_6/16.66% C_2H_4/16.66% C_3H_8/air mixtures. Fig. 6(b) shows that the addition of pure C_3H_8 to $CH_4/C_2H_6/C_2H_4$ ternary blends becomes an important source of methyl radicals produced from the β-scission of $n\dot{C}_3H_7$ radicals, is responsible for the slower reactivity of the quaternary blends compared to the ternary blends at higher temperatures.

Fig. 7(a) shows that at lower temperature the reactivity of the quaternary blends is governed by $C_3H_8 + \dot{O}H \leftrightarrow n\dot{C}_3H_7 + H_2O$ being the most reactivity promoting channel, while the most sensitive reactions inhibiting the reactivity are $C_3H_8 + \dot{O}H \leftrightarrow i\dot{C}_3H_7 + H_2O$ and $n\dot{C}_3H_7O_2 \leftrightarrow C_3H_6 + H\dot{O}_2$. At T_C < 900 K, $n\dot{C}_3H_7$ radicals add to molecular oxygen producing n-propyl-peroxy ($nC_3H_7\dot{O}_2$) radicals, which then isomerize to hydroperoxyl-propyl ($\dot{C}_3H_6OOH1\text{–}3$) radicals that can add to molecular oxygen generating hydroperoxyl-propyl-peroxy ($C_3H_6OOH1\text{–}3\dot{O}_2$) radicals. The $C_3H_6OOH1\text{–}3\dot{O}_2$ radicals can further isomerize and generate a carbonyl hydroperoxide and an $\dot{O}H$ radical. Finally, the carbonyl hydroperoxide undergoes RO–OH bond cleavage, producing a second $\dot{O}H$ radical and a carbonyl-alkoxy ($R\dot{O}$) radical in a chain branching process that increases the reactivity of propane at low temperatures, Fig. 6(a). The addition of propane to the ternary blends significantly increases the reactivity of the 50% CH_4/16.66% C_2H_6/16.66% C_2H_4/16.66% C_3H_8 quaternary blends, this being just less reactive than the pure C_3H_8/'air' mixture at lower temperatures (< 900 K), Fig. 5(a).

4.3. Effect of pressure on ignition

Fig. 9 illustrates the effect of the pressure on IDTs for 50% CH_4/25% C_2H_4/25% C_2H_6 blend, 50% CH_4/16.66% C_2H_4/16.66% C_2H_6 /16.66% C_3H_8 blend along with pure methane at $\varphi = 1.0$. Fig. 9 indicates that the reactivity of the mixtures increases at high-pressure conditions due to the corresponding increase in concentration with pressure. Furthermore, it is observed that at lower temperatures (< 830 K), the addition of C_2H_4/C_2H_6 and $C_2H_4/C_2H_6/C_3H_8$ fuels to pure methane for the ternary and quaternary blends, results in faster IDTs at high-pressure conditions (20, 40 and 80 atm) compared to the 1 atm case. Figs. 10(a) and 10(b) illustrate the effect of pressure on IDTs based on reaction path analyses depicted by black numbers for the 1 atm case and blue numbers for the 40 atm case at 800 K for the 50% CH_4/25% C_2H_4/25% C_2H_6 and 50% CH_4/16.66% C_2H_4/16.66% C_2H_6/16.66% C_3H_8 blends, respectively. The flux analyses presented in Figs. 10(a) and 10(b) show that for the ternary and quaternary blends, the total fluxes going through the ignition promoting pathways $\dot{C}H_3 + O_2 \leftrightarrow CH_3\dot{O}_2$ and $\dot{C}H_3 + H\dot{O}_2 \leftrightarrow CH_3\dot{O} + \dot{O}H$ are around two times higher at 40 and 80 atm compared to 1 atm, while ~32% less flux goes through the methyl radical recombination reaction $\dot{C}H_3 + \dot{C}H_3 (+M) \leftrightarrow C_2H_6 (+M)$ at 40 and 80 atm compared to 1 atm, thus increasing the overall reactivity of the blends at high pressure and low-temperature conditions. Moreover, for the ternary blend, as pressure rises, the carbon fluxes going through the channels generating hydroxyl–ethyl ($\dot{C}_2H_4OH$) radicals from $C_2H_4 + \dot{O}H$ followed by the O_2 addition and the subsequent dissociation of $O_2\dot{C}_2H_4OH$ leading to two formaldehyde and a hydroxyl radical increases, as seen in Fig. 10(a). These formaldehyde molecules react with $H\dot{O}_2$ radicals to generate H_2O_2, which more strongly promotes the reactivity through the thermal dissociation reaction $H_2O_2 (+M) \leftrightarrow \dot{O}H + \dot{O}H (+M)$ at the high-pressure condition of 40 and 80 atm compared to 1 atm, as shown in Fig. S53.

For the 50% CH_4/16.66% C_2H_4/16.66% C_2H_6 /16.66% C_3H_8 quaternary blend, at 1 atm, a considerable amount of $n\dot{C}_3H_7$ (21.7%) undergoes β-scission, via $n\dot{C}_3H_7 \leftrightarrow \dot{C}H_3 + C_2H_4$, while for 40 atm, the percentage contribution through this channel reduces significantly accounting only 0.4% of the total flux. Whereas, at 40 atm ~34% more flux goes through the $n\dot{C}_3H_7 + O_2 \leftrightarrow nC_3H_7\dot{O}_2$ pathway compared to 1 atm condition increasing the reactivity for the quaternary blend at high pressures and low temperatures through the generation of two reactive $\dot{O}H$ radicals, as discussed in Section 4.2.

4.4. Correlation analysis

Reliable global correlations that can accurately reproduce experimental measurements are desirable tools for analytical, semi-empirical, or computational fluid dynamics (CFD) calculations of reactive flows. Such correlations are versatile tools that can predict a mixture's sensitivity to any change in the correlated parameters. As discussed previously [2, 3], these correlations significantly reduce the required simulation time in response to any change in the chemical system, a critical parameter in real-time combustion controlling and monitoring systems. A simple form of the correlations applied here follows those previously published [2, 3] and is expressed in Eqn. (3). As previously shown, this type of correlation can reasonably explain the IDT characteristics of single and binary blended C_1 – C_3 hydrocarbons over a wide range of conditions [2, 3]. Here, it should be noted that Eqn. (3) explains the general form of the correlations used in the study so that the "F" variable is zero for the tertiary blended C_1 – C_2 fuels where no propane is present.

$$\tau_{corr} = 10^{A}\exp\left(\frac{B}{T_C}\right)[CH_4]^{C}[C_2H_4]^{D}[C_2H_6]^{E}[C_3H_8]^{F}[oxygen]^{G}[diluent]^{H} \quad (3)$$

where A represents the pre-exponential factor coefficient, B represents the activation energy divided by universal gas constant, and C – H represent coefficients for methane, ethylene, ethane, propane, oxidizer, and dilution, respectively.

All of the correlations were derived using NUIGMech1.2 based on thousands of adiabatic constant volume simulations, and their corresponding correlation coefficients are presented below and in Tables S12 – S15 of the Supplementary material. The correlation coefficients were calculated using a non-linear curve fitting routine available in OriginPro 8.5 [45] which provides linear regressions together with residuals, R^2, χ^2 and standard errors for every coefficient value. Some of the examples of these conditions

are presented in Fig. 5(b) and Fig. 9. However, according to the simple form of Eqn. (3), the correlations are derived over ranges where the dependency of the IDT on the various parameters does not become highly non-linear. Moreover, for relatively long IDTs (> 10 ms) measured using the RCM, the correlation results derived using the adiabatic constant volume calculations differs significantly from the simulations including heat loss effects for the facility. We have already discussed this effect in detail [2,4].

For $1100 \leq T_C \leq 2000$ K:

$$\tau_{corr} = 10^{-10.94}\exp\left(\frac{2,120,8}{T_C}\right)[CH_4]^{1.004}[C_2H_4]^{-0.888} [C_2H_6]^{-0.041}[C_3H_8]^{0.0}[\text{oxygen}]^{-1.399}[\text{diluent}]^{0.666} \quad (4)$$

$$\tau_{corr} = 10^{-10.36}\exp\left(\frac{2,132,0}{T_C}\right)[CH_4]^{0.834}[C_2H_4]^{-0.222} [C_2H_6]^{-0.186}[C_3H_8]^{-0.165}[\text{oxygen}]^{-1.496}[\text{diluent}]^{0.48} \quad (5)$$

For $800 \leq T_C \leq 1100$ K:

$$\tau_{corr} = 10^{-8.049}\exp\left(\frac{1,681,7}{T_C}\right)[CH_4]^{0.31}[C_2H_4]^{-0.722} [C_2H_6]^{-0.138}[C_3H_8]^{0.0}[\text{oxygen}]^{-0.398}[\text{diluent}]^{-0.162} \quad (6)$$

$$\tau_{corr} = 10^{-8.011}\exp\left(\frac{1,582,6}{T_C}\right)[CH_4]^{0.133}[C_2H_4]^{-0.257} [C_2H_6]^{-0.105}[C_3H_8]^{-0.5}[\text{oxygen}]^{-0.292}[\text{diluent}]^{-0.089} \quad (7)$$

At high temperatures (1100 – 2000 K), the coefficient associated with CH_4 in both blends ($CH_4/C_2H_4/C_2H_6$/'air' and $CH_4/C_2H_4/C_2H_6/C_3H_8$/'air') is strongly positive, while those for C_2H_4, C_2H_6, and C_3H_8 are negative. CH_4 produces high concentrations of $\dot{C}H_3$ radicals, which are relatively less reactive compared to $\dot{H}$ atoms produced in the oxidation of C_2H_4, C_2H_6, and C_3H_8. Thus, increasing the CH_4 concentration in the ternary and quaternary blends will increase IDT, and increasing C_2H_4, C_2H_6, and C_3H_8 concentrations will decrease the mixture IDT. Moreover, the coefficient associated with C_3H_8 in the quaternary ($CH_4/C_2H_4/C_2H_6/C_3H_8$/'air') blend is smaller than the coefficients for C_2H_4 and C_2H_6. This is because, at high temperatures, C_3H_8 produces $\dot{C}H_3$ radicals and C_2H_4 molecules from $n\dot{C}_3H_7$ radicals that decompose via β-scission reaction by $n\dot{C}_3H_7 \leftrightarrow C_2H_4 + \dot{C}H_3$, whereas C_2H_4 and C_2H_6 oxidation produces higher amounts of $\dot{H}$ atoms, thus more effectively enhancing the reactivity of the C_2H_4 or C_2H_6 blended mixtures than those of the C_3H_8 blended ones. Therefore, although increasing the concentrations of C_2H_4 and C_3H_8 relative to CH_4 will increase mixture reactivity, the former will dominate the latter.

Furthermore, at high temperatures, the coefficient corresponding to the oxidizer is significantly higher than other coefficients showing the strong sensitivity of oxygen concentrations under the respective conditions. For the low-temperature range, 800 – 1100 K, the coefficients for C_2H_4 and C_3H_8 become strongly negative. This is because, in this temperature range, C_2H_4 and C_3H_8 greatly enhance reactivity by producing higher concentrations of highly active $\dot{O}H$ radicals compared to the CH_4 and C_2H_6 fuels. Moreover, the coefficient corresponding to the oxidizer in Eqns. (6) and 7 is comparable to other coefficients showing less importance on oxygen concentrations under these specific conditions. A more detailed correlation table is included for all conditions studied in this work as Supplemental material, which includes the coefficients, standard errors related to coefficients R^2, and χ^2. For both, low and high temperatures, the corresponding R^2 and χ^2 parameters are ranging from 0.985 – 0.999 and 1.53×10^{-4} – 1.02×10^{-11}, respectively.

Figures S51 and S52 in the Supplementary material compare the predictions of the quaternary correlations derived in this study with our prior published experimental IDTs of binary blends for C_2H_4/C_3H_8 and C_2H_6/C_3H_8 mixtures at high temperature and high-pressure conditions [4]. The present correlations are also compared with the IDT predictions calculated using the binary correlations derived in our previous work [4]. It can be seen that the global correlation of the quaternary blend is unable to accurately predict the IDTs of the C_2H_4/C_3H_8 and C_2H_6/C_3H_8 binary blends. This is attributed to the fact that the present correlations were derived from simulations of quaternary mixtures with CH_4 as the major fuel component. Eq. (5) shows that, for quaternary mixtures, the coefficient associated with CH_4 is strongly positive compared to the other fuel components in the blend and thus CH_4 dominates the predicted reactivity of the fuel mixture. Since our previously published [4] binary blends did not include CH_4 as an additive component, the predictions of the present correlations differ significantly from those calculated using the binary mixture correlations [4].

Conclusions

In the current study, a detailed experimental and kinetic modeling study of the IDT characteristics of C_1 – C_3 novel ternary and quaternary blends of $CH_4/C_2H_4/C_2H_6$ and $CH_4/C_2H_4/C_2H_6/C_3H_8$ mixtures was performed over a wide range of experimental conditions, temperature (~750 – 2000 K), pressure (1 – 135 bar), equivalence ratio ($0.5 \leq \varphi \leq 2.0$), and dilution (~75 – 90%). 24 new IDT datasets, including approximately 360 data points were measured, which were not already available in the literature. Low- and high-temperature IDT characteristics of $CH_4/C_2H_4/C_2H_6$ and $CH_4/C_2H_4/C_2H_6/C_3H_8$ combinations were investigated using the ST and RCM facilities at NUIG and PCFC RWTH Aachen University. The results showed that NUIGMech1.2 could predict the IDT characteristics of the blends studied with high fidelity over the wide range of conditions studied here.

Therefore, NUIGMech1.2 was used to perform studies on the blending and pressure effect on ignition. It was observed that for all blends used in this work, as the temperature and the pressure increase, the IDTs decrease. For high temperatures ($T >$ 1100 K), CH_4 exhibit the slowest reactivity because its chemistry is mainly driven by methyl chemistry, $\dot{C}H_3 + H\dot{O}_2 \leftrightarrow CH_4 + O_2$, and $\dot{C}H_3 + \dot{C}H_3\ (+M) \leftrightarrow C_2H_6\ (+M)$; these reaction pathways are responsible for the very slow ignition on pure CH_4 and the ternary and quaternary blends at this temperature. C_2H_6 is the second-fastest mixture to ignite, and this is because the pressure dependant reaction from ethyl radical enhances the reactivity $\dot{C}_2H_5\ (+M) \leftrightarrow C_2H_4 + \dot{H}\ (+M)$ at the same time, competition with the concerted elimination reaction $\dot{C}_2H_5 + O_2 \leftrightarrow C_2H_4 + H\dot{O}_2$ slow down the ignition making C_2H_6 slower than C_2H_4. C_2H_4 mixtures show the fastest reactivity due to the vinyl ($\dot{C}_2H_3$) chemistry that makes C_2H_4 the fastest fuel to ignite. Furthermore, C_3H_8 is much slower than C_2H_4 due to the high amount of methyl ($\dot{C}H_3$) radicals produced from $n\dot{C}_3H_7$ channels.

It was observed that for low temperatures ($T <$ 1100 K), methyl chemistry is still responsible for the slow ignition exhibited by CH_4. This is because of the large amount of $\dot{C}H_3$ radicals reacting with O_2 to form methyl peroxy radicals $\dot{C}H_3 + O_2 \leftrightarrow CH_3\dot{O}_2$, which further react through $CH_3\dot{O}_2 + CH_3\dot{O}_2 \leftrightarrow CH_3\dot{O} + CH_3\dot{O} + O_2$ to inhibit the reactivity. However, here C_2H_6 is the second slowest due to the concerted elimination reaction, $C_2H_5\dot{O}_2 \leftrightarrow C_2H_4 + H\dot{O}_2$, which becomes very important at this temperature. Additionally, C_2H_4 is the second-fastest in igniting due to hydroxy–ethyl-peroxy ($\dot{O}_2C_2H_4OH$) and oxirane (C_2H_4O1–2) channels that enhance the reactivity. Moreover, C_3H_8 exhibits the fastest ignition at this temperature due to the considerable amount of $\dot{O}H$ radicals generated

by the addition of *n*-propyl ($n\dot{C}_3H_7$) radicals to O_2 and going to chain branching reactions.

Finally, several correlations were derived from mimicking the performance of NUIGMech1.2 in predicting the IDT characteristics of the blended fuels over a wide range of pressure, temperature, equivalence ratio, fuel composition, and dilution. The results demonstrated that the derived correlations could be depended upon as agile, fast, and reasonably reliable tools to predict the IDTs of the blends studied over their validity range of pressure, temperature, and mixture composition.

Fig. 2

Supplementary files

All supplementary files are attached to the online version of the article.

1. The Supporting Information file; including all referred items and plots in the manuscript.

2. The Supplementary files (.zip); including all raw data such as datasheets and oscilloscopes voltage and pressure traces etc.

Declaration of Competing Interest

The authors declare that they have no known competing financial interests or personal relationships that could have appeared to influence the work reported in this paper.

Acknowledgements

The authors would like to express their gratitude to Shell Research Ltd. and Science Foundation Ireland (SFI) for funding via project numbers 15/IA/3177 and 16/SP/3829, and KAY-ICHEC via the project ngche079c. The authors from PCFC, RWTH Aachen University, would like to recognize the funding support from the German Research Foundation (Deutsche Forschungsgemeinschaft, DFG) through project number – 322460823 (HE7599/2-1).

Supplementary materials

Supplementary material associated with this article can be found, in the online version, at doi:10.1016/j.combustflame.2021.111626.

References

[1] C.J. Aul, W.K. Metcalfe, S.M. Burke, H.J. Curran, E.L. Petersen, Ignition and kinetic modeling of methane and ethane fuel blends with oxygen: a design of experiments approach, Combust. Flame 160 (2013) 1153–1167.

[2] M. Baigmohammadi, V. Patel, S. Martinez, S. Panigrahy, A. Ramalingam, U. Burke, K.P. Somers, K.A. Heufer, A. Pekalski, H.J. Curran, A comprehensive experimental and simulation study of ignition delay time characteristics of single fuel C1−C2 hydrocarbons over a wide range of temperatures, pressures, equivalence ratios, and dilutions, Energy Fuels 34 (3) (2020) 3755–3771.

[3] M. Baigmohammadi, V. Patel, S. Nagaraja, A. Ramalingam, S. Martinez, S. Panigrahy, A.A. El–Sabor Mohamed, K.P. Somers, U. Burke, K.A. Heufer, A. Pekalski, H.J. Curran, Comprehensive experimental and simulation study of the ignition delay time characteristics of binary blended methane, ethane, and ethylene over a wide range of temperature, pressure, equivalence ratio, and dilution, Energy Fuels 34 (7) (2020) 8808–8823.

[4] S. Martinez, M. Baigmohammadi, V. Patel, S. Panigrahy, A.B. Sahu, S.S. Nagaraja, A. Ramalingam, A.A. El-Sabor Mohamed, K.P. Somers, K.A. Heufer, A. Pekalski, H.J. Curran, An experimental and kinetic modeling study of the ignition delay characteristics of binary blends of ethane/propane and ethylene/propane in multiple shock tubes and rapid compression machines over a wide range of temperature, pressure, equivalence ratio, and dilution, Combust. Flame 228 (2021) 401–414.

[5] P.J. Ross, Taguchi Techniques for Quality Engineering, McGraw-Hill, New York, 1988.

[6] E.L. Petersen, M.J.A. Rickard, M.W. Crofton, E.D. Abbey, M.J. Traum, D.M. Kalitan, A facility for gas- and condensed-phase measurements behind shock waves, Meas. Sci. Technol. 16 (2005) 1716–1729.

[7] B.W. Weber, C.J. Sung, M.W. Renfro, On the uncertainty of temperature estimation in a rapid compression machine, Combust. Flame 162 (2015) 2518–2528.

[8] A. Ramalingam, K. Zhang, A. Dhongde, L. Virnich, H. Sankhla, H. Curran, A. Heufer, An RCM experimental and modeling study on CH4 and CH4/C2H6 oxidation at pressures up to 160 bar, Fuel 206 (2017) 325–333.

[9] A.A. El-Sabor Mohamed, S. Panigrahy, A. Sahu, G. Bourque, H.J. Curran, An experimental and modeling study of the auto-ignition of natural gas blends containing C1–C7 n-alkanes, Proc. Combust. Inst. 38 (2021) 365–373.

[10] S.S. Nagaraja, J. Power, G. Kukkadapu, S. Dong, S..W. Wangon, W.J. Pitz, H.J. Curran, A single pulse shock tube study of pentene isomer pyrolysis, Proc. Combust. Inst. 38 (2021) 881–889.

[11] S. Panigrahy, J. Liang, S. Nagaraja, Z. Zuo, G. Kim, T. MacDougall, S..S. Vasu, H.J. Curran, A comprehensive experimental and improved kinetic modeling study on the pyrolysis and oxidation of propyne, Proc. Combust. Inst. 38 (2021) 479–488.

[12] S. Dong, K. Zhang, P.K. Senecal, G. Kukkadapu, S.W. Wagnon, S. Barrett, N. Lokachari, S. Panigrahy, W.J. Pitz, H.J. Curran, A comparative reactivity study of 1-alkene fuels from ethylene to 1-heptene, Proc. Combust. Inst. 38 (2021) 611–619.

[13] S.S. Nagaraja, J. Liang, S. Dong, S. Panigrahy, A. Sahu, G. Kukkadapu, S.W. Wagnon, W.J. Pitz, H.J. Curran, A hierarchical single-pulse shock tube pyrolysis study of C2–C6 1-alkenes, Combust. Flame 219 (2020) 456–466.

[14] A. Ramalingam, S. Panigrahy, Y. Fenard, H. Curran, K.A. Heufer, A chemical kinetic perspective on the low-temperature oxidation of propane/propene mixtures through experiments and kinetic analyses, Combust. Flame 223 (2021) 361–375.

[15] D.G. Goodwin, R.L. Speth, H.K. Moffat, B.W. Weber, Cantera: an object-oriented software toolkit for chemical kinetics, Thermodyn. Transp. Processes (2018) https://www.cantera.org, doi:10.5281/zenodo.170284.

[16] Reaction-design, CHEMKIN-PRO 18.2, San Diego, 2013.

[17] C.J. Sung, H.J. Curran, Using rapid compression machines for chemical kinetics studies, Prog. Energ. Combust. 44 (2014) 1–18.

[18] S.S. Goldsborough, S. Hochgreb, G. Vanhove, M.S. Wooldridge, H.J. Curran, C.J. Sung, Advances in rapid compression machine studies of low- and intermediate-temperature autoignition phenomena, Prog. Energy Combust. Sci. 63 (2017) 1–78.

[19] U. Burke, K.P. Somers, P. O'Toole, C.M. Zinner, N. Marquet, G. Bourque, E.L. Petersen, W.K. Metcalfe, Z. Serinyel, H.J. Curran, An ignition delay and kinetic modeling study of methane, dimethyl ether, and their mixtures at high pressures, Combust. Flame 162 (2015) 315–330.

[20] E.E. Dames, A.S. Rosen, B.W. Weber, C.W. Gao, C.-J. Sung, W.H. Green, A detailed combined experimental and theoretical study on dimethyl ether/propane blended oxidation, Combust. Flame 168 (2016) 310–330.

[21] S. Chih-Jen, H.J. Curran, Using rapid compression machines for chemical kinetics studies, Prog. Energy Combust. Sci. 44 (2014) 1–18.

[22] V. Gururajan, F.N. Egolfopoulos, Direct sensitivity analysis for ignition delay times, Combust. Flame 209 (2019) 478–480.

[23] W.K. Metcalfe, S.M. Burke, S.S. Ahmed, H.J. Curran, A hierarchical and comparative kinetic modeling study of C1−C2 hydrocarbon and oxygenated fuels, Int. J. Chem. Kinet. 45 (2013) 638–675.

[24] S.M. Burke, W. Metcalfe, O. Herbinet, F. Battin-Leclerc, F.M. Haas, J. Santner, F.L. Dryer, H.J. Curran, An experimental and modeling study of propene oxidation. Part 1: speciation measurements in jet-stirred and flow reactors, Combust. Flame 161 (2014) 2765–2784.

[25] S.M. Burke, U. Burke, R. Mc Donagh, O. Mathieu, I. Osorio, C. Keesee, A. Morones, E.L. Petersen, W. Wang, T.A. DeVerter, M.A. Oehlschlaeger, B. Rhodes, R.K. Hanson, D.F. Davidson, B.W. Weber, C.-J. Sung, J. Santner, Y. Ju, F.M. Haas, F.L. Dryer, E.N. Volkov, E.J.K. Nilsson, A.A. Konnov, M. Alrefae, F. Khaled, A. Farooq, P. Dirrenberger, P.-A. Glaude, F. Battin-Leclerc, H.J. Curran, An experimental and modeling study of propene oxidation. part 2: ignition delay time and flame speed measurements, Combust. Flame 162 (2015) 296–314.

[26] Y. Li, C.W. Zhou, K.P. Somers, K. Zhang, H.J. Curran, The oxidation of 2-butene: a high pressure ignition delay, kinetic modeling study and reactivity comparison with isobutene and 1-butene, Proc. Combust. Inst. 36 (2017) 403–411.

[27] C.W. Zhou, Y. Li, U. Burke, C. Banyon, K.P. Somers, S. Ding, S. Khan, J.W. Hargis, T. Sikes, O. Mathieu, E.L. Petersen, M. AlAbbad, A. Farooq, Y. Pan, Y. Zhang, Z. Huang, J. Lopez, Z. Loparo, S.S. Vasu, H.J. Curran, An experimental and chemical kinetic modeling study of 1,3-butadiene combustion: ignition delay time and laminar flame speed measurements, Combust. Flame 197 (2018) 423–438.

[28] H. Hashemi, J.G. Jacobsen, C.T. Rasmussen, J.M. Christensen, P. Glarborg, S. Gersen, M. van Essen, H.B. Levinsky, S.J. Klippenstein, High-pressure oxidation of ethane, Combust. Flame 182 (2017) 150–166.

[29] G. Bagheri, E. Ranzi, M. Pelucchi, A. Parente, A. Frassoldati, T. Faravelli, Comprehensive kinetic study of combustion technologies for low environmental impact: MILD and OXY-fuel combustion of methane, Combust. Flame 212 (2020) 142–155.

[30] Chemical-kinetic mechanisms for combustion applications. 2012. http://combustion.ucsd.edu.

[31] G.P. Smith, D.M. Golden, M. Frenklach, N.W. Moriarty, B. Eiteneer, M. Goldenberg, C.T. Bowman, R.K. Hanson, S. Song, W.C. Gardiner, V.V. Lissianski, Z. Qin, (1999). http://www.me.berkeley.edu/gri_mech/..

[32] G.P. Smith, Y. Tao, H. Wang, Foundational Fuel Chemistry Model Version 1.0 (FFCM-1), Stanford University, 2016.

[33] A.W. Jasper, S.J. Klippenstein, L.B. Harding, Theoretical rate coefficients for the reaction of methyl radical with hydroperoxyl radical and for methylhydroperoxide decomposition, Proc. Combust. Inst. 32 (2009) 279–286.

[34] R. Zhu, C. Lin, The CH3 + HO2 reaction: first-principles prediction of its rate constant and product branching probabilities, J. Phys. Chem. A 105 (2001) 6243–6248.

[35] S.M. Villano, L.K. Huynh, H.-.H. Carstensen, A.M. Dean, High-pressure rate rules for alkyl + O2 reactions. 1. The dissociation, concerted elimination, and iso-

merization channels of the alkyl peroxy radical, J. Phys. Chem. A 115 (2011) 13425–13442.
[36] U. Burke, K.P. Somers, P. O'Toole, C.M. Zinner, N. Marquet, G. Bourque, E.L. Petersen, W.K. Metcalfe, Z. Serinyel, H.J. Curran, An ignition delay and kinetic modeling study of methane, dimethyl ether, and their mixtures at high pressures, Combust. Flame 162 (2015) 315–330.
[37] I.R. Slagle, D. Gutman, J.W. Davies, M.J. Pilling, Study of the recombination reaction CH3+CH3 –>C2H6 Part 1. Experiment, J. Phys. Chem. 92 (1988) 2455–2462.
[38] M. Sangwan, C. Yan, E.N. Chesnokov, L.N. Krasnoperov, Reaction CH3 + CH3 → C2H6 studied over the 292–714K temperature and 1–100bar pressure ranges, J. Phys. Chem. A 119 (2015) 7847–7857.
[39] K. Glänzer, M. Quack, J. Troe, High temperature UV absorption and recombination of methyl radicals in shock waves, Sympos. (Int.) Combust. 16 (1977) 949–960.
[40] M.A. Blitz, N.J.B. Green, R.J. Shannon, M.J. Pilling, P.W. Seakins, C.M. Western, S.H. Robertson, Reanalysis of rate data for the reaction CH3 + CH3 → C2H6 using revised cross sections and a linearized second-order master equation, J. Phys. Chem. A 119 (2015) 7668–7682.
[41] B. Wang, H. Hou, L.M. Yoder, J.T. Muckerman, C. Fockenberg, Experimental and theoretical investigations on the methyl−methyl recombination reaction, J. Phys. Chem. A 107 (2003) 11414–11426.
[42] S.J. Klippenstein, Y. Georgievskii, L.B. Harding, Predictive theory for the combination kinetics of two alkyl radicals, Phys. Chem. Chem. Phys 8 (2006) 1133–1147.
[43] P.D. Lightfoot, P. Roussel, F. Caralp, R. Lesclaux, Flash photolysis study of the CH_3O_2 + CH_3O_2 and CH_3O_2 + HO_2 reactions between 600 and 719 k: unimolecular decomposition of methylhydroperoxide, J. Chem. Soc. Faraday Trans. 87 (19) (1991) 3213–3220.
[44] M. Keiffer, A.J. Miscampbell, M.J. Pilling, A global technique for analysing multiple decay curves application to the CH_3 + O_2 system, J. Chem. Soc., Faraday Trans. 2 (1988) 505–514.
[45] Origin(Pro), Version 8.5. OriginLab Corporation, Northampton, MA, USA, 2013.